iScience

CellPress
OPEN ACCESS

Article

Physiological and transcriptomic responses of *Chlorella sorokiniana* to ciprofloxacin reveal molecular mechanisms for antibiotic removal

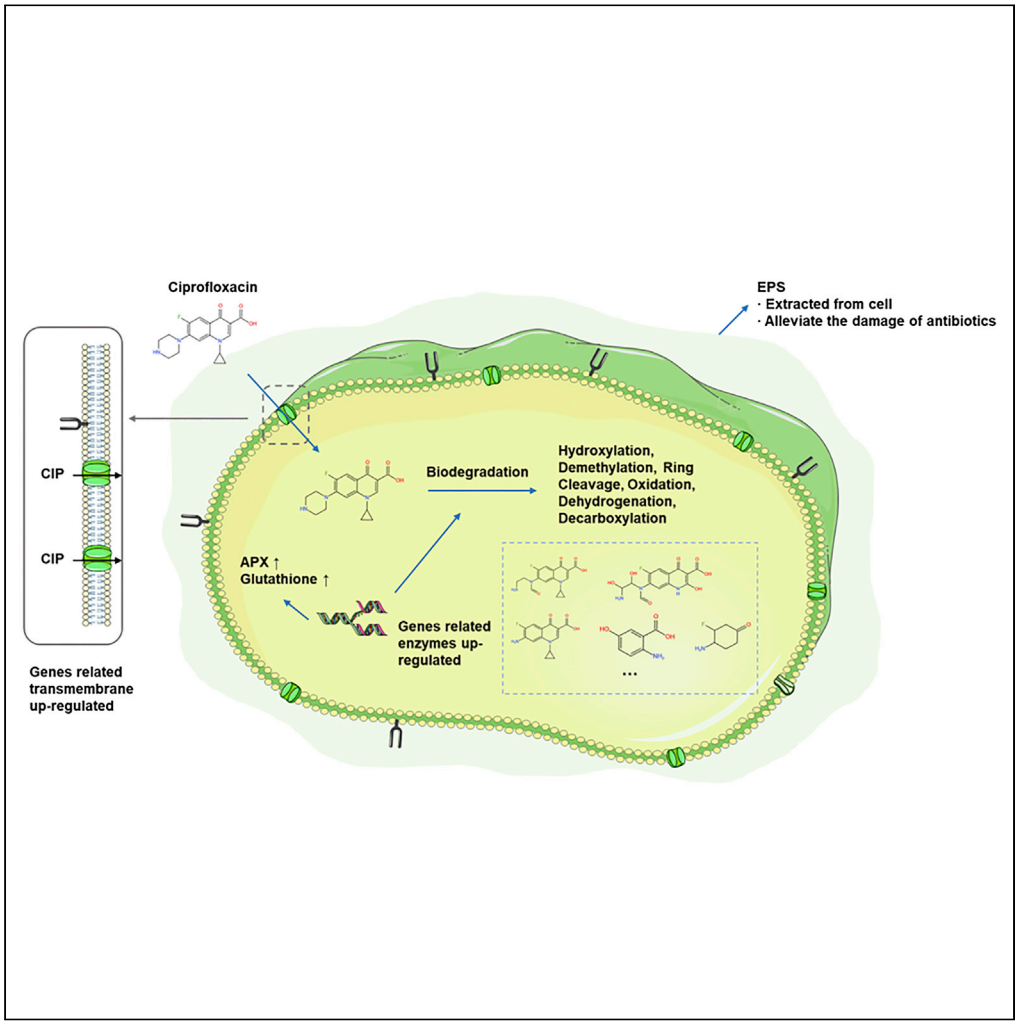

Zhuo Li, Shuangxi Li, Tianrui Li, Xinxin Gao, Liandong Zhu

ldzhu@whu.edu.cn

Highlights

Freshwater microalgae *Chlorella sorokiniana* was exposed to ciprofloxacin

Microalgae released humic-like substances to alleviate the damage

The maximum removal of ciprofloxacin was 83.3% under 20 mg L^{-1} CIP exposure

Ciprofloxacin could be biodegraded with the help of intracellular oxidoreductases

Li et al., iScience *25*, 104638
July 15, 2022
https://doi.org/10.1016/j.isci.2022.104638

iScience

CellPress
OPEN ACCESS

Article

Physiological and transcriptomic responses of *Chlorella sorokiniana* to ciprofloxacin reveal molecular mechanisms for antibiotic removal

Zhuo Li,[1] Shuangxi Li,[1] Tianrui Li,[1] Xinxin Gao,[1] and Liandong Zhu[1,2,*]

SUMMARY

Microalgae-based technology is an effective and environmentally friendly method for antibiotics-contaminated wastewater treatment. To assess the tolerance and removal ability of *Chlorella sorokiniana* to ciprofloxacin (CIP), this study comprehensively revealed the responses of *C. sorokiniana* to CIP exposure and its degradation processes through physiological and transcriptomic analyses. Although the photosynthetic system was inhibited, the growth of *C. sorokiniana* was not negatively affected by CIP. Dissolved organic matter was analyzed and indicated that humic-like substances were released to alleviate the stress of CIP. In addition, the maximum removal of CIP was 83.3% under 20 mg L^{-1} CIP exposure. HPLC-MS/MS and RNA-Seq analyses suggested that CIP could be bioaccumulated and biodegraded by *C. sorokiniana* through the reactions of hydroxylation, demethylation, ring cleavage, oxidation, dehydrogenation, and decarboxylation with the help of intracellular oxidoreductases, especially cytochrome P450. Collectively, this research shows that *C. sorokiniana* have a great potential for removing CIP from wastewater.

INTRODUCTION

Fluoroquinolones (FQs), as a class of common antibiotics, are usually used to treat respiratory, urinary and skin infections in humans and animals (Van Doorslaer et al., 2014). As a third-generation fluoroquinolone, ciprofloxacin (CIP) is frequently detected in the environment, and its concentration could reach up to 31 mg L^{-1} in pharmaceutical wastewater effluent (Larsson et al., 2007), 14 mg L^{-1} in municipal wastewater effluent (Fick et al., 2009) and 5.02 mg L^{-1} in surface water (Gothwal and Shashidhar, 2017). The emerging occurrence of CIP might persistently affect the growth, reproduction and survival of aquatic organisms, causing the severe problems for human beings (Westerhoff et al., 2005). In addition, the existence of antibiotics in the environment can also induce the development and dissemination of antibiotic resistance (Rodriguez-Mozaz et al., 2015). Therefore, it is imperative to develop effective strategies to reduce CIP discharges into the aquatic environment.

Some non-biotic processes such as the photocatalytic degradation process and advanced oxidation processes can efficiently remove CIP (Chen et al., 2022; Kumar et al., 2022; Phoon et al., 2020). However, because of the high operational and system maintenance costs, these physicochemical methods might have a low viability from the commercial perspective (Homem and Santos, 2011). Microalgae, as a species for a cost-effective and environmentally friendly treatment process, have exhibited a high potential for antibiotic removal (Aron et al., 2021; Cheah et al., 2018; Xie et al., 2019). Zhou et al. (2014) used four freshwater green microalgae (*Chlamydomonas reinhardtii*, *Scenedesmus obliquus*, *Chlorella pyrenoidosa* and *Chlorella vulgaris*) to remove metals and pollutants including CIP, and clearly demonstrated the capability of the microalgae to remove most of the selected antibiotics. Recently, Peng et al. (2022) investigated the performance and mechanism of levofloxacin removal by *Chromochloris zofingiensis* in heterotrophic mode, reaching 79%–95% removal efficiency under different concentrations of levofloxacin. Xie et al. (2020) demonstrated that *Chlamydomonas* sp. Tai-03 was capable of efficient removal of CIP by biodegradation (65%) and photolysis (35%). There are two pathways considered for possible contribution in antibiotic removal. On the one hand, microalgae can act as photosensitizers to promote the indirect photolysis of antibiotics through the excretion of extracellular organic matter (Wei et al., 2021). On the other hand, antibiotics can enter the cell by adsorption and transmembrane transport and are decomposed into small

[1]School of Resources & Environmental Science, Hubei International Scientific and Technological Cooperation Base of Sustainable Resource and Energy, Hubei Key Laboratory of Biomass-Resources Chemistry and Environmental Biotechnology, Wuhan University, Wuhan 430079, P.R. China

[2]Lead contact

*Correspondence: ldzhu@whu.edu.cn

https://doi.org/10.1016/j.isci.2022.104638

molecules by intracellular oxidoreductases (Xiong et al., 2018). However, such observations are still limited for some wastewater microalgae such as *C. sorokiniana*, which is fast-growing with efficient nutrient removal abilities for wastewater treatment operations.

In general, the toxicological effects of CIP on microalgae are closely related to their species. Cyanobacteria are particularly susceptible to antibiotics, taking an example that the concentration for 50% of maximal effect (EC_{50}) of *Synechocystis* sp. against CIP was 39 μg L^{-1} (You et al., 2021). In contrast, eukaryotic algae are generally less affected by CIP. Nie et al. (2008) investigated the response of *C. vulgaris* to CIP exposure, and proved that the growth of *C. vulgaris* was inhibited by CIP under all concentrations, and the inhibition efficiency raised from 9.2% to 72.4% when the concentration ranged from 2.0 to 31.25 mg L^{-1} after 96-h exposure. Hagenbuch and Pinckney (2012) found that the half-max inhibitory concentrations (IC_{50}) of CIP to two species of marine diatoms, *Cylindrotheca closterium* and *Navicula ramosissima* were 55.43and 72.12 mg L^{-1}, respectively. Xiong et al. (2017) found that *Chlamydomonas mexicana* showed an evident growth inhibition only under concentrations higher than 40 mg L^{-1} of CIP. In addition, a recent study showed that the 72h- and 96h-IC_{50} values of CIP for *Chlorella* sp. were 15.11 and 2.92 mg L^{-1}, respectively (Gomaa et al., 2021). However, it is still not clear about the performance of such wastewater microalgae *C. sorokiniana* under CIP exposure from the viewpoint of physiological and transcriptomic responses. Therefore, more investigation is required to explore the response mechanisms and tolerance of such microalgae to CIP exposure, as well as the main mechanisms of the degradation process of CIP and the organism activities involved.

To summarize, previous studies mainly focus on the removal performances of microalgae to treat antibiotics including CIP; however, the knowledge of relative growth and stress responses was still limited. In addition, some reported studies pay more attention to the toxic effects of CIP on microalgae, whereas the degradation of CIP and the corresponding mechanisms are still unknown in literature. In this study, culture growth, photosynthetic system and extracellular polymers alterations were examined to investigate the physiological and transcriptomic influences of different CIP concentrations on *C. sorokiniana*. Meanwhile, the removal efficiencies of CIP under different concentrations were also determined and the according proportion of photolysis, hydrolysis and biodegradation was analyzed. Notably, with the help of high-performance liquid chromatography-tandem mass spectrometry (HPLC-MS/MS), CIP elimination routes and degradation mechanisms were comprehensively investigated. Subsequently, RNA-sequencing analysis of *C. sorokiniana* was performed under different CIP concentrations. Based on transcriptomic responses, the physiological alterations in microalgae were fully explained. Therefore, this research will provide deep insights to understand the responses of microalgae upon exposure to CIP and form a foundation to recognize the biodegradation process of CIP in microalgae, thus facilitating the development and practical application of microalgae for wastewater treatment, especially for those containing antibiotics.

RESULTS AND DISCUSSION

C. sorokiniana growth analysis

The effects of CIP on *C. sorokiniana* growth were evaluated during the cultivation of 10 days. As shown in Figure 1A and Table S1, the dry weight of *C. sorokiniana* had no significant ($p < 0.05$) difference between four experimental groups and control group, indicating that the growth of *C. sorokiniana* was not affected by CIP stress. The specific growth rate (shown in Figure 1B) proved this conclusion, with no difference between the groups from the overall viewpoint, except for the day 3 when microalgae might have adapted to the growth environment with a sudden burst of growth. Similar findings were also seen in other studies on the effects of CIP on the growth of microalgae such as *Chlamydomonas* sp. Tai-03 (Xie et al., 2020). The results provided good supporting evidence for *C. sorokiniana* to treat CIP, while the growth of such organisms for the treatment of CIP was also not inhibited in other studies (Xiong et al., 2017).

Photosynthetic parameters analysis

Photosynthetic pigments, as important photosynthetic substances in microalgae, play essential roles in a series of vital photosynthetic processes, like light capture, energy absorption and transformation. The chlorophyll contents of *C. sorokiniana* were investigated on the 10^{th} day to determine the effect of CIP on photosynthetic pigments. As shown in Figures 2A, a significant positive correlation between chlorophyll *a* content and CIP concentration was observed, whereas there was no significant difference on chlorophyll *b* content in the presence of any CIP concentration. As the concentration of CIP increased from 0 to 20 mg

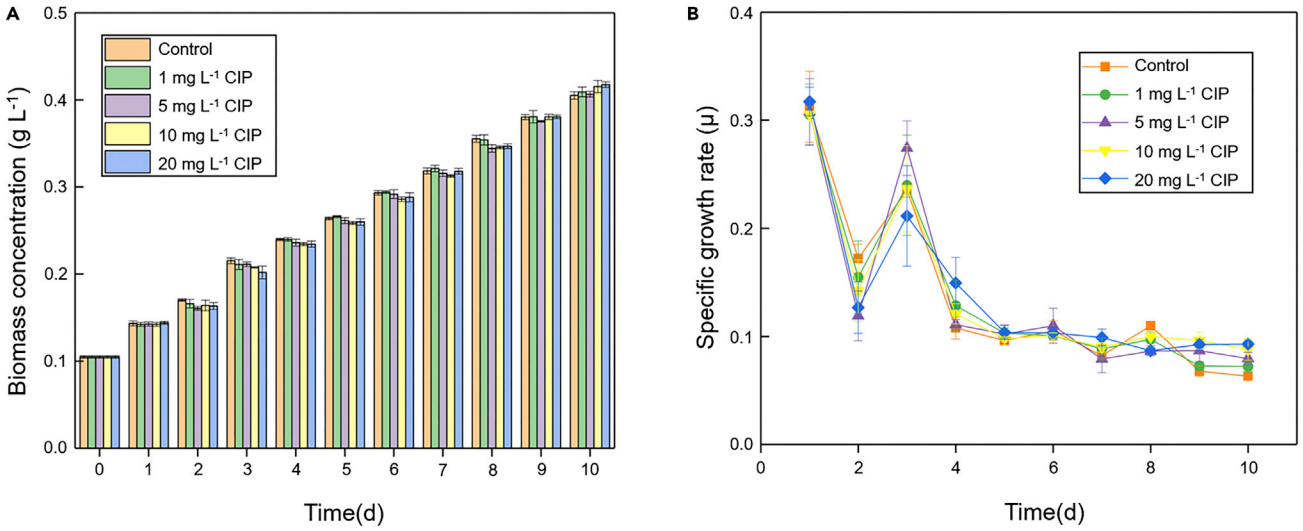

Figure 1. The growth of *C. sorokiniana* under CIP exposure

Effects of CIP on *C. sorokiniana* growth in terms of dry weight (A) and specific growth rate (μ) (B) with different concentrations of CIP (0, 1, 5, 10 and 20 mg L^{-1}) during 10 days of cultivation. Error bars represent SD(n = 3).

L^{-1}, the chlorophyll *a* content increased from 5.45 to 7.90 mg g^{-1}, while the chlorophyll *b* content only increased from 1.62 to 2.18 mg g^{-1}. Besides, carotenoid contents also increased slightly, although there was no significant difference between groups with the CIP concentrations of 0 and 1, 5 and 10 mg L^{-1}.

The variability of photosynthetic pigments' contents visually reflected the photosynthetic activity of *C. sorokiniana*. Because of its sensitivity to growth conditions, nutrient availability and various abiotic stresses, PSII efficiency is employed to evaluate the stress response of microalgae (Lovyagina and Semin, 2016). As a rapid and non-invasive technology, chlorophyll fluorescence test is widely used to assess the performance of PSII under different conditions (Kumar et al., 2014). Therefore, the effects of CIP on *C. sorokiniana* in terms of ecological physiology and toxicology were measured by chlorophyll a fluorescence transient on days 0, 2, 4, 6, 8, and 10, respectively. As shown in Figures 2B and Table S2, the Fv/Fm values of the control group increased slightly from 0.63 to 0.69, whereas the maximum Fv/Fm value of the test group at 20 mg L^{-1} CIP concentration reached 0.73. However, the results of day 10 indicated that the maximal photosynthetic efficiency of *C. sorokiniana* showed no significant differences as the increase of CIP concentration, which is consistent with the analysis of microalgae growth. On the other hand, OEC values, described in Figure 2C, presented an opposite pattern to Fv/Fm values, with a slow decrease with time, except for a slight recovery on the 10^{th} day. Meanwhile, the value of OEC obviously decreased as the CIP concentrations increased. OEC, as one of the most sensitive components in the photosynthetic electron transport chain, reflected the state of water photooxidation in photosynthetic organisms (Gomes et al., 2017). The decreased efficiency of the OEC indicated that CIP impaired the water-splitting apparatus.

As shown in Figure 2D, when exposed to 0, 1, 5, 10 and 20 mg L^{-1} CIP, the ΦPSII of *C. sorokiniana* gradually decreased from 0.937 to 0.753 on day 10. At the same time, Figure 2D demonstrated that the experimental groups with different concentrations of CIP caused an evident decrease in ΦPSII, compared to the control group, where there was no significant change in ΦPSII within 10 days. ΦPSII reduction would alter the photochemistry and electron transport of PSII, which is associated with energy dissipation through regulated and unregulated non-photochemical pathways (Juneau et al., 2002). NPQ results in Figure 2E proved that the non-photochemical quenching was inhibited by the addition of CIP. As the most important photoprotective mechanism, NPQ is triggered by the high pH gradient (ΔpH) across the thylakoid membrane induced by high light irradiation (Lambrev et al., 2012). Therefore, the decrease of ΦPSII and NPQ suggested that CIP toxicity affected the mechanism of fluorescence quenching by non-photochemical processes. Besides, although PSII reaction center was damaged, induced by impaired PSII-associated electron transport, the synthesis of photosynthetic pigments was still stimulated, which was also observed in *C. sorokiniana* exposed to free nitrous acid (Abbew et al., 2021).

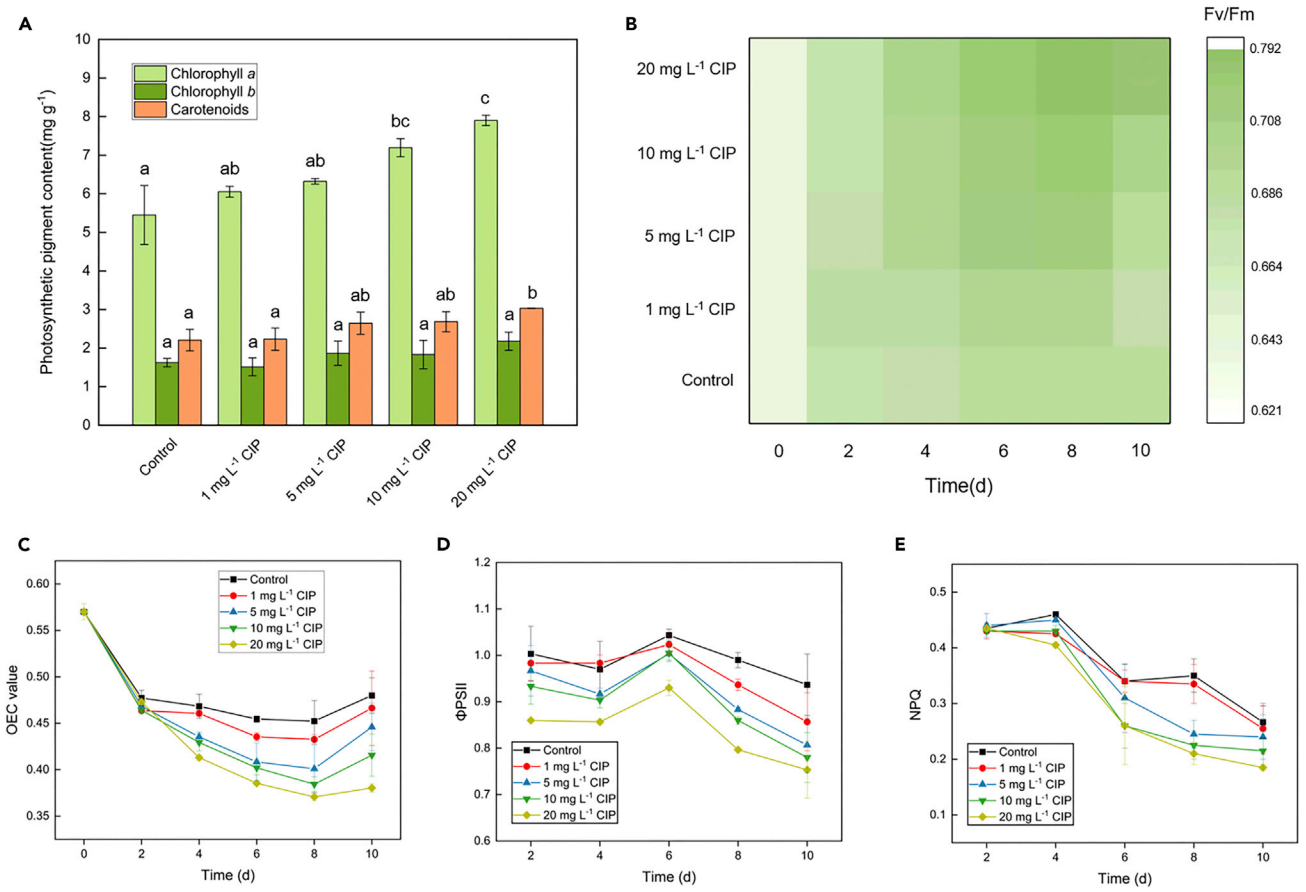

Figure 2. The photosynthetic parameters of *C. sorokiniana* under CIP exposure

Effects of CIP on *C. sorokiniana* photosynthetic pigments (A) and parameters as indicated by Fv/Fm (B), OEC value (C), ΦPSII (D) and NPQ (E) with different concentrations of CIP at 0, 1, 5, 10 and 20 mg L^{-1} during 10 days of cultivation. Error bars represent SD(n = 3). The different letters indicate significant differences ($p < 0.05$) between the control and experimental treatments.

DOM analysis

DOM characterization analysis

Secreted by organisms, DOM content variation is commonly considered to contribute to microbial activity (He et al., 2018; Zhao et al., 2018). In the present study, the EEM spectra of DOM released by *C. sorokiniana* at different CIP concentrations was measured using EEM-PARAFAC. Three components of DOM were identified based on the PARAFAC model using OpenFluor database, as described in Figure 3. Component C1 (emission maximum 419 nm with 330 and 265 nm excitation maxima) was considered to be a fulvic acid-type component, which is reported as a ubiquitous matter found in almost all environments (Amaral et al., 2020; Yamashita et al., 2011). Another humic-like component C3 had an emission maximum at 478 nm and two excitation maxima (260 and 355–365 nm), possibly corresponding to the microbial humic-like components on the basis of the results of Yamashita et al. (Bistarelli et al., 2021; Yamashita et al., 2011). Component C2, on the other hand, had emission/excitation maxima at 338 nm and 280 nm, respectively, and was strongly characterized as the amino acid tryptophan, reflecting recent biological production (Brym et al., 2014).

Fluorescent components and indices analysis

The maximum fluorescence intensity (F_{max}) of the three identified components in the present study of EEM-PARAFAC models was shown in Figures 4A, 4B, and 4C. It was indicated that the F_{max} of Component C1 (fulvic acid-type component) increased markedly as the increase of CIP concentration, and the value upsurged from 0.43 to 2.02 with CIP concentrations range from 0 to 5 mg L^{-1} and slowly rose to 2.56 as the increase of CIP concentration to 20 mg L^{-1}. In addition, Component C2, amino acid tryptophan

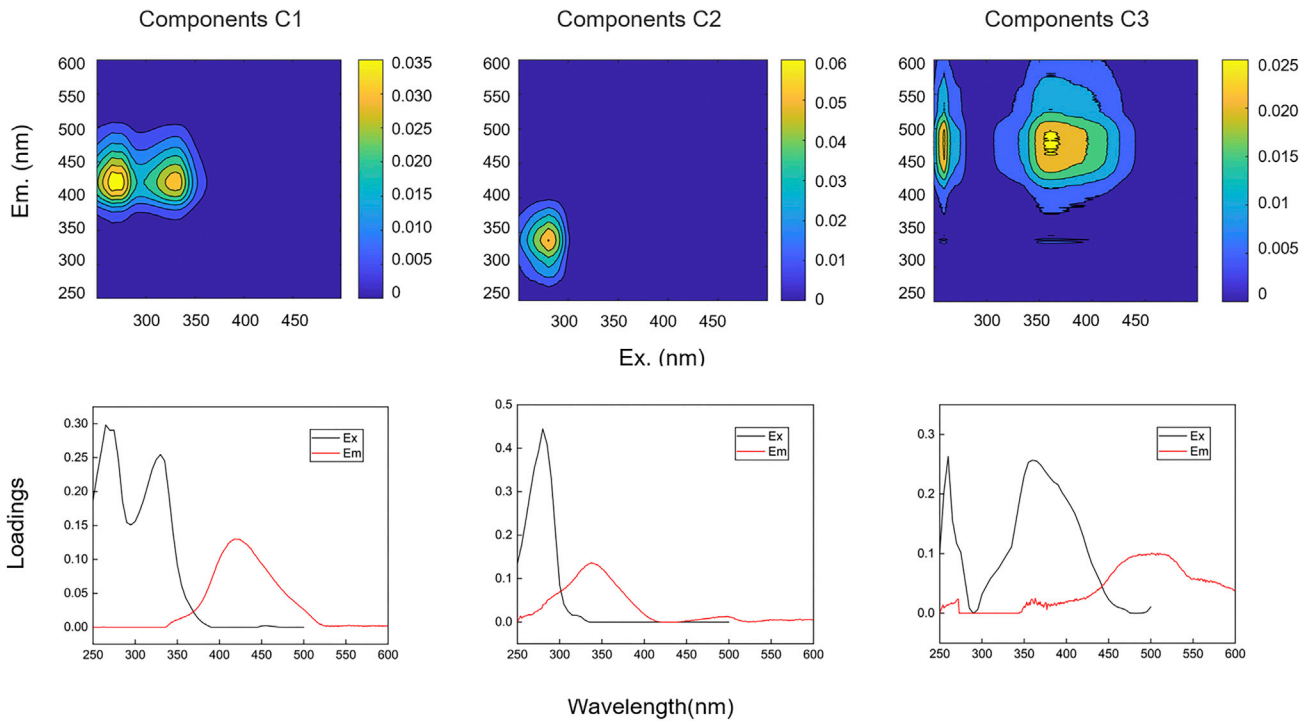

Figure 3. The three fluorescent components (Components 1, 2 and 3) identified by the PARAFAC model

substances, decreased approximately 35.4% as the increase of CIP concentration. Humic-like substances C3 experienced a fluctuating upward tendency, as shown in Figure 4C. Changes in extracellular secretions were in part a response of *C. sorokiniana* to the stress of CIP. Humic acid had been proved to possess binding plots for FQs, specifically the CIP, the aromatic ring of which was highly affected (Zhao et al., 2019). The increased level of this substance in DOM might explain why the growth of *C. sorokiniana* was not affected under CIP stress in this study. Tryptophan, as one precursor to the synthesis of ultraviolet-absorbing secondary metabolites such as scytonemin, could relatively avoid harmful effects of long-term UV radiation exposure (Xu et al., 2013). To a certain extent, its reduction in DOM led to the damage of the photosynthetic system of *C. sorokiniana*.

Figures 4D and 4E indicated the disparities of biological index (BIX) and humic index (HIX) of experimental groups based on EEM spectra. BIX and HIX are complementary tools and are particularly suitable for the determination of DOM origin and aging in a simple and fast manner. In this study, BIX showed downward trends ranging from 0.97 to 0.33 in all treatments, whereas HIX showed converse trends ranging from 0.46 to 0.80. BIX is introduced to determine the characteristic of biological activity (Huguet et al., 2009), and higher HIX values indicate a deeper humification degree and higher humic acid content (Du et al., 2021). The shift in the values of these two parameters indicated that the productivity of *C. sorokiniana* was reduced under stress. However, HIX still remained low (<1) compared to another study (Jia et al., 2017b), indicating that microbial metabolic activity remained at a relatively high level.

Analysis of CIP removal

CIP removal efficiency of C. sorokiniana

The removal of CIP by *C. sorokiniana* was investigated on a daily basis during the exposure period. The maximal removal efficiency of CIP was 83.30% at CIP concentration of 20 mg L^{-1} (Figure 5A), indicating that *C. sorokiniana* had a great potential to remove CIP at a relatively high concentration. However, only 16.69%, 17.13% and 59.83% removal efficiencies were achieved for treatments with the CIP concentration of 1, 5 and 10 mg L^{-1}, respectively. The analysis of the removal efficiency also revealed an interesting phenomenon that the CIP degradation efficiency by *C. sorokiniana* increased as the increase of pollutant concentrations, especially for the treatment with 20 mg L^{-1} CIP, achieving 76.06% removal efficiency within two days. The finding was in accordance with the study of Cheng et al. 2017, 2018, who found that the

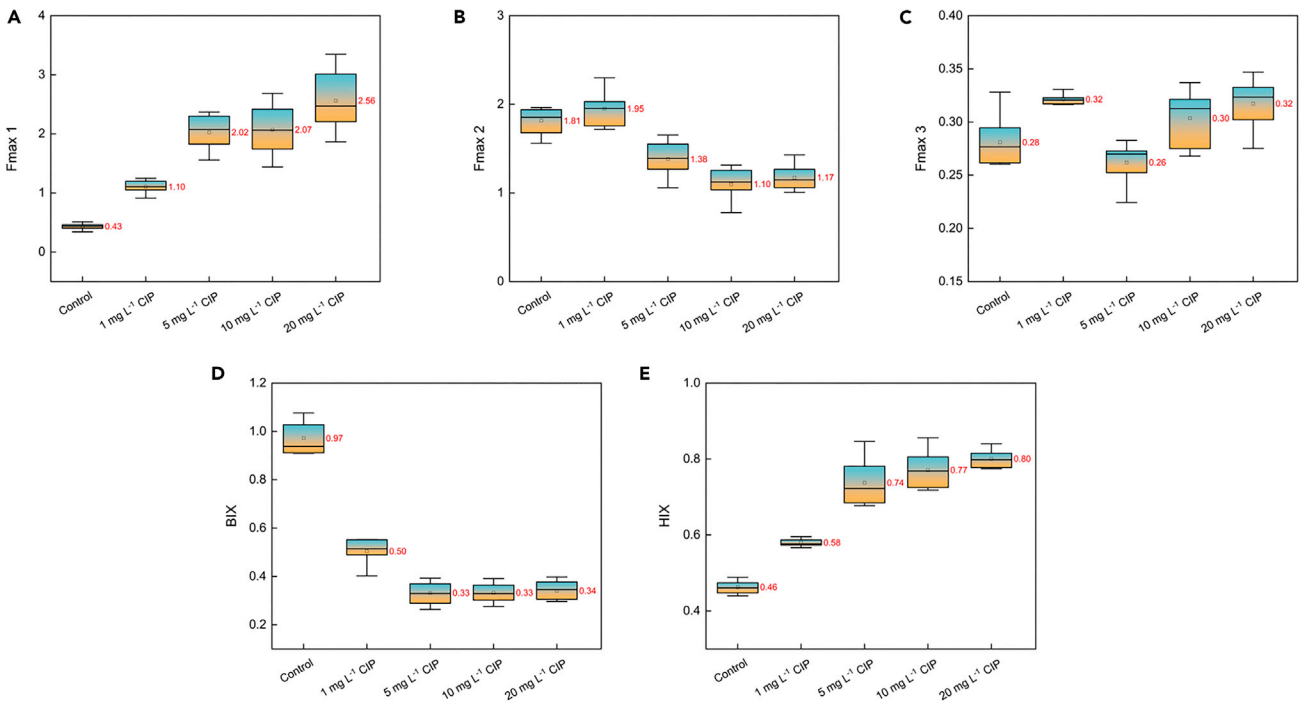

Figure 4. Box-whisker plot of the maximum fluorescence (Fmax) for the three fluorescence components and FI, HIX, BIX in five groups
(A) Comp 1, (B) Comp 2, (C) Comp 3, (D) BIX, (E) HIX.

degradation efficiency of *Chlorella* PY-ZU1 for tilmicosin and ethinyl estradiol increased as the increase of pollutant concentrations. However, the reason for such a large difference between the different groups in this study might be because of the stress expression of *C. sorokiniana*. In addition, the removal of CIP by *C. sorokiniana* might begin with the adsorption and transmembrane transport of CIP, ending with intracellular redox. It was more difficult for *C. sorokiniana* to adsorb CIP under a lower concentration, resulting in a lower removal efficiency.

Analysis of elimination routes

In general, the removal of CIP occurs via three main routes, including hydrolysis, photolysis and bioremoval (Oberoi et al., 2019; Xiao et al., 2021; Xiong et al., 2018). In this study, the degradation pathway of CIP at 20 mg L^{-1} was analyzed (Figure 5B). Owing to the hydrophobic characteristic of CIP, only 3.28% was removed by hydrolysis, whereas the photolysis of CIP accounted for 6.28% of removal. In summary, bioremoval remained the dominant pathway for CIP degradation by *C. sorokiniana*, accounting for 73.73% of the total removal, which confirmed that *C. sorokiniana* had great potential to treat high concentrations of CIP. It should be noted that because photolysis and hydrolysis were analyzed independently, their efficiency increased despite the fact that the total degradation efficiency remained almost constant.

The photolysis and biodegradation pathway of CIP

As shown in Figure 6 and Table S3, five intermediates were identified for the CIP photolysis process. The results indicated that oxidation in the piperazine ring was the main photocatalytic degradation pathway. This is in accordance with a recent study where it was found that piperazine ring oxidation was an important pathway of CIP elimination in neutral or alkaline solution (Li et al., 2020b). On the one hand, the intermediate product *m/z* 261 was formed by the dealkylation in the piperazine ring of *m/z* 304. On the other hand, the attack by hydroxyl radicals in solution caused the conversion of compound *m/z* 304 to *m/z* 286 by the defluorination process. In this pathway, the fluoroquinolone ring in the molecules of *m/z* 360, *m/z* 332, *m/z* 304, *m/z* 286 and *m/z* 261 remained intact. Similar intermediates were also found in photocatalytic degradation in the UVA/TiO_2 system, graphite felt anodic oxidation and ozonation (Lu et al., 2020; Chen et al., 2021; Li and Hu, 2018).

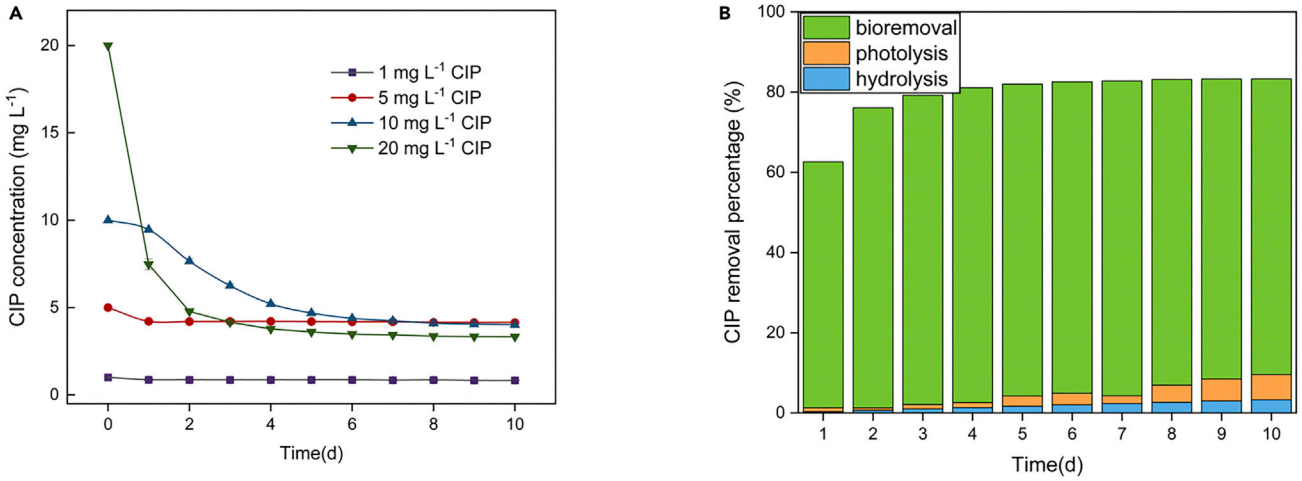

Figure 5. CIP removal and elimination routes by *C. sorokiniana*

CIP removal at 1, 5, 10 and 20 mg L^{-1} during 10 days of degradation with error bars representing SD(n = 3) (A). And time course profiles of different elimination routes of 20 mg L^{-1} CIP with the percentage of biodegradation, biosorption, photolysis and hydrolysis during the CIP removal process (B).

In addition, eleven intermediates were determined during CIP biodegradation. Two intermediates, *m/z* 332 and *m/z* 261, were also detected in the photolysis process, indicating that oxidation and dealkylation in piperazine played equally important roles in biodegradation. Furthermore, the quinolone structure of CIP, including cyclopropyl group and quinolone ring, could be destroyed during the biodegradation process because of various oxidoreductases in microalgae. As shown in Figure 6, *m/z* 324 was generated by the direct loss of cyclopropyl and attack of hydroxyl radicals of *m/z* 332, in which hydroxylases secreted by cells were crucial. On the basis of *m/z* 332, the breakage of the carbon-carbon double bond formed the intermediate *m/z* 272, and further formed *m/z* 216 by decarboxylation. After dehydrogenation and deamination, *m/z* 216 was converted into cyclohexane substance *m/z* 174, which could be decarboxylated to form *m/z* 130. Finally, *m/z* 130 would open the ring to form alkane substance *m/z* 182, which would be oxidized to CO_2 and H_2O by cells. Meanwhile, deamination and hydroxylation induced the formation of *m/z* 262 from *m/z* 261. In addition, after the cyclopropane group on the *m/z* 262 was removed, *m/z* 190 could be produced by the addition of a methyl group, as previously reported, and the carbon-carbon double bond in *m/z* 262 was simultaneously opened by oxygenase. m/z 190 experienced the removal of ketone groups and the action of oxygenase to form the final product *m/z* 152.

In this study, biodegradation mechanisms for CIP and the differences between photolysis and biodegradation processes were clearly demonstrated. The piperaquine ring and the fluorine atom might both be removed by either photolysis or biodegradation process. Cyclopropyl, which was generally difficult to be destroyed in photolysis, was removed by various enzymatic reactions in the biodegradation process. At the same time, the carboxyl and ketone groups on the structure of quinolone were also certainly removed during the biodegradation process. The roles of these moieties in antibacterial activity have been described in other studies. For example, cyclopropyl was part of the enzyme-DNA binding complex with a hydrophobic interaction with DNA (Ma et al., 1999). The F atom could boost the antibacterial activity of CIP, and the loss of fluorine proved that the toxicity was reduced to microalgal cells (Chen et al., 2021; Maia et al., 2014). The opening of the epoxide ring and carbon-carbon double bond might also indicate that hydroxylase, oxidase and oxygenase were involved in biodegradation of CIP.

Transcriptome sequencing and analysis

A comparative transcriptome analysis was performed through RNA-seq, to further explore the molecular mechanisms acting in *C. sorokiniana* in response to CIP stress. Nine cDNA libraries involving the three treatment groups were constructed from three biological replicates of *C. sorokiniana* treated with Col (without CIP), CIP+ (5 mg L^{-1} CIP), CIP++ (20 mg L^{-1} CIP). The total number of transcripts was 140,019, 9526 unigenes of which were assembled. All of the above high-quality unigenes experienced annotation analysis and 8005 unigenes were identified via Gene Ontology (GO).

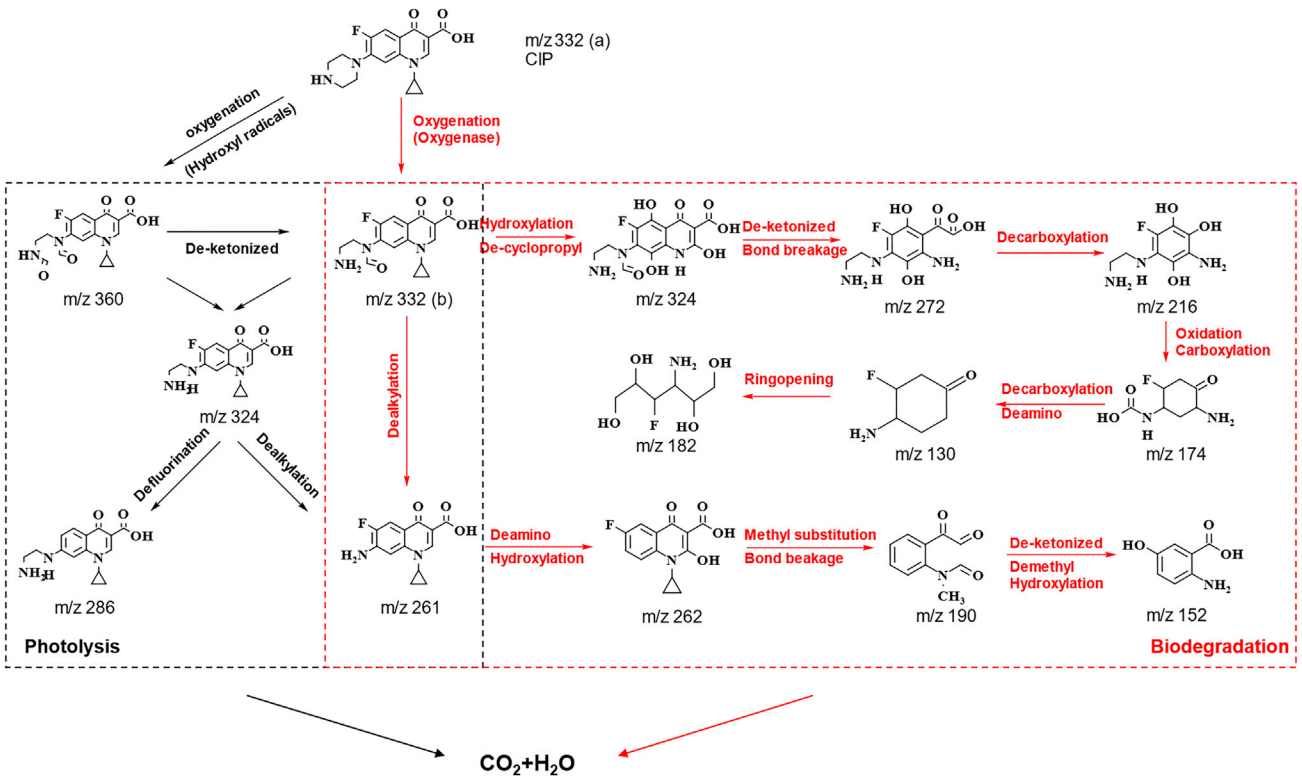

Figure 6. Proposed degradation pathway for CIP photolysis (black box) and biodegradation (red box) by *C. sorokiniana*

TPM values were used to quantify the expression levels of all the identified unigenes. The median and quartile values of differential gene expression are shown in Figure 7A. By the methods previously described, DE-Gs were easily identified between the CIP treatments and the control (CIP+/Col and CIP++/Col). As shown in Figure 7B, there were a total of 334 DE-Gs in CIP+/Col, in which 164 were upregulated and 170 were downregulated. In contrast, there existed a total of 427 DE-Gs in CIP++/Col, where 247 were upregulated and 180 were downregulated. The above results indicated that a high concentration of CIP (CIP++) not only resulted in more DE-Gs in total, but also induced more upregulated genes than downregulated genes. Venn diagram (Figure 7C) was constructed to analyze the common and specific DE-Gs under CIP stress. Based on these DE-Gs, genes that potentially responded to CIP stress specificity in *C. sorokiniana* were functionally identified.

Functional analysis of DE-Gs

Differentially expressed genes in CIP+/Col and CIP++/Col were compared and functionally annotated by the GO functional annotation classification system, and classified in 38 terms of three clusters including 12 in biological processes, 13 in cellular components and 13 in molecular functions (shown in Table S4). CIP, transported from the outside to the inside of the microalgae cell, could be catabolized by the enzymatic reaction of *C. sorokiniana*. Meanwhile, the biological processes of *C. sorokiniana* also needed to be regulated to survive under CIP stress. Therefore, in the follow-up analysis, genes related stimulus response, photosystem, transmembrane activity and metabolism of substances and energy were analyzed.

Differentially expressed genes related to stimulus response

In general, the concentration of reactive oxygen species in microalgae cells would increase under environmental stress, probably resulting in cell death (Liao et al., 2015). Thus, DE-Gs associated with reactive oxygen species (ROS) partially reflected the oxidative damage received by the cells. The expression of ascorbate peroxidase (APX), one of antioxidative enzymes, significantly increased 4.76 times in CIP++/Col, whereas no difference was found in CIP+/Col (shown in Table 1) (Yun et al., 2019). Simultaneously, the expression of genes related to glutathione, one of nonenzymatic antioxidants (Kusvuran, 2021), increased 3.86 times in CIP++/Col. Considering the growth of microalgae in this study, it can be concluded that

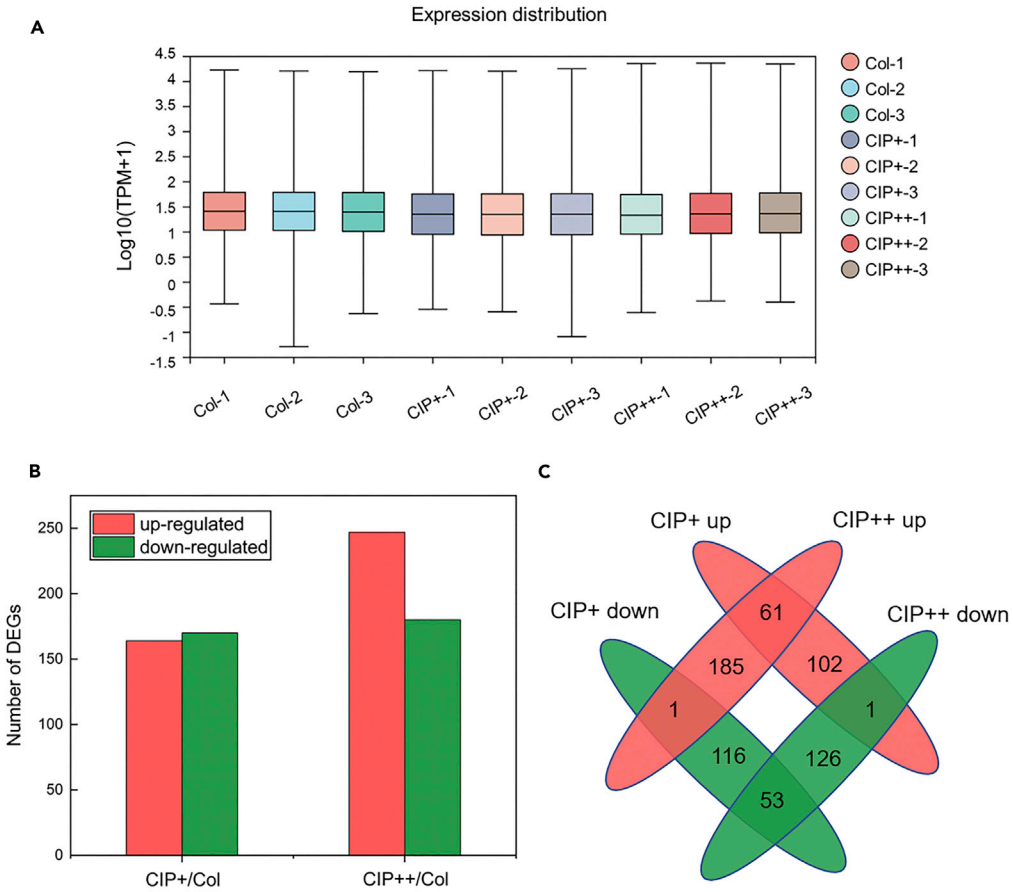

Figure 7. DEGs of *C. sorokiniana* under CIP exposure

High-throughput RNA sequencing (RNA-seq) analysis of DE-Gs in the roots of *C. sorokiniana* exposed to CIP stress. *C. sorokiniana* was treated with 0, 10, and 20 mg L^{-1} CIP for 10 days for RNA-seq with three biological replicates per CIP concentration. Boxplots of TPM values in log10-scale in different samples showing the distribution of these values about the median (A). Three biological replicates were set in 0 mg L^{-1} CIP treatment group (Col-1; Col-2; Col-3), 10 mg L^{-1} CIP treatment group (CIP + -1; CIP + -2; CIP + -3) and 20 mg L^{-1} CIP treatment group (CIP++-1; CIP++-2; CIP++-3). And the number of DE-Gs between control and CIP treatment groups (B) and venn diagrams of the DE-Gs (C).

oxidative stress would not be induced by a low CIP concentration. However, the synthesis of antioxidant substances would be enhanced to eliminate the ROS in the cells and prevent the microalgae cells from oxidative damage in the face of a high CIP concentration. Multidrug resistant genes, i.e., DETOXIFICATION 16-like (gene-C2E21_4753), pleiotropic drug resistance 1 (gene-C2E21_1044) and multidrug resistance-associated 1 (gene-C2E21_0081), played an important role in the drug-resistance of *C. sorokiniana* through the promotion of the discharge of exogenous pollutants into the extracellular compartment (Tang et al., 2021).

Differentially expressed genes related to photosystem

The increased chlorophyll contents were supported by the observed upregulation of chlorophyll-binding or biosynthesis-associated genes in *C. sorokiniana*. For example, coproporphyrinogen III oxidase chloroplast precursor, as one of the most important enzymes of chlorophyll synthesis (Santana et al., 2002), accordingly overexpressed 3.47 and 2.33 times in treatment CIP+/Col and CIP++/Col. Delta-aminolevulinic acid dehydratase, which is related to the synthesis of porphobilinogen as one type of chlorophyll-a intermediate (Abbew et al., 2021), was evidently increased 2.25 times in treatment CIP+/Col. Meanwhile, gene related to chlorophyllide a oxygenase activity (gene-C2E21_1445) was found to be upregulated in

Table 1. Differentially expressed genes related to stimulus response of *C. sorokiniana* induced by CIP

	CIP+/Col		CIP++/Col		CIP++/CIP+		
Gene ID	log2Fold change	Fold change	log2Fold change	Fold change	log2Fold change	Fold change	Annotations
gene-C2E21_5809	–	–	1.17	2.25 (up)	–	–	ascorbate peroxidase
gene-C2E21_4135	–	–	1.04	2.06 (up)	1.15	2.21 (up)	S-formylglutathione hydrolase
gene-C2E21_6607	–	–	1.72	3.29 (up)	1.88	3.69 (up)	2-cys peroxiredoxin
gene-C2E21_2197	1.14	2.21 (up)	–	–	–	–	2-cys peroxiredoxin BAS1
gene-C2E21_3071	1.12	2.18 (up)	1.15	2.21 (up)	–	–	Hydroxylamine reductase
gene-C2E21_0778	1.41	2.66 (up)	1.29	2.44 (up)	–	–	Hydroxylamine reductase
gene-C2E21_4753	–	–	1.10	2.15 (up)	1.31	2.48 (up)	DETOXIFICATION 16-like
gene-C2E21_1044	2.28	4.86 (up)	1.59	3.01 (up)	–	–	Pleiotropic drug resistance 1
gene-C2E21_0081	1.72	3.29 (up)	–	–	–	–	multidrug resistance-associated 1 isoform X8
gene-C2E21_5810	−1.14	2.20 (down)	–	–	–	–	L-ascorbate peroxidase 6 isoform X1 isoform A

"-" indicated "P-adjust > 0.05" or "not significantly different expressed" or "|log2FC|<1".

treatment CIP++/Col. In addition, genes related to carotenoid biosynthesis were found to be overexpressed in both groups. The increased pigment content might be an attempt to mitigate oxidative stress.

The DE-Gs associated with photosynthetic system II were also listed in Table 2. The response of microalgae in the face of different levels of CIP stress was different. For treatment CIP+/Col, gene related to photosystem II repair were upregulated, whereas the structural function of chloroplasts was not greatly affected. However, genes related to chloroplast photosynthetic function were obviously upreguated or downregulated in treatment CIP++/Col. The precursor processing gene of D1 protein, which constituted the heterodimer core of Photosystem II (PSII) with the D2 protein and was related to photodamage repair (Antonacci et al., 2020; Tian et al., 2021), was evidently dwonregulated 2.15 times in treatment CIP++/Col. Meanwhile, the downregulated genes also encompassed protein subunits involved in photosynthetic electron transfer such as Cyt *b6*/f complex subunits and ferredoxin (5.38 and 2.36, respectively). Thus, the cells' regulation mechanism resulted in a 4.35-fold overexpression of the gene encoding thioredoxin in treatment CIP++/Col, and other studies also demonstrated that thioredoxin was effective in preventing chlorophyll degradation and promoting biomass increase (Zhang et al., 2020). In addition, the expression of chlorophyll *a*/b-binding protein, an antenna protein (Adamiec et al., 2015), was also affected by the stress of CIP. In summary, it is the co-expression of these DE-Gs that caused the photosynthetic system to exhibit differences, as described in the photosynthetic parameters analysis.

Differentially expressed genes related to transmembrane activity

Differentially expressed genes related to CIP transport were shown in Table 3. The expression of two ABC transporters genes (gene-C2E21_3505 and gene-C2E21_147) was 2.53 and 2.06 times higher in treatment CIP++/Col, which might be responsible for CIP transport as they showed no differences in treatment CIP+/Col. Similar findings for the function of ABC transports were also seen in other studies, where distinctive drugs were found to be involved in the transmembrane transport of polycyclic aromatic hydrocarbons (PAHs) (Stingley et al., 2004). In particular, in an early proteomics study in the investigation of the effects of FQs on *Pseudomonas aeruginosa*, Zhou et al. found that the ABC transporter was expressed in CIP-intermediate and -resistant strains but not in the sensitive strain (Zhou et al., 2006), which provided certain explanations for the effective removal of CIP only at high concentrations in this study. Notably, the expression of zinc ion-related transporter proteins (gene-C2E21_1856, gene-C2E21_6330 and gene-C2E21_8904) was positively correlated with the concentration of CIP. As an important enzyme cofactor for RNA polymerase, Zn(II) is closely associated with protein synthesis, which might promote the cellular synthesis of enzymes related to the removal of CIP (Li et al., 2020d). Besides, Zn(II) also promoted the synthesis of copper-zinc superoxide dismutase, which defended against oxidative stress for cells (Wang et al., 2019), whereas genes associated with the transporter protein of copper element were obviously upregulated

Table 2. Differentially expressed genes related to photosystem of *C. sorokiniana* induced by CIP

	CIP+/Col		CIP++/Col		CIP++/CIP+		
Gene ID	log2Fold change	Fold change	log2Fold change	Fold change	log2Fold change	Fold change	Annotations
gene-C2E21_2115	1.80	3.47 (up)	1.22	2.33 (up)	–	–	coproporphyrinogen III oxidase chloroplast precursor
gene-C2E21_1445	–	–	1.07	2.11 (up)	–	–	Elongation factor P, chlorophyllide a oxygenase [overall] activity
gene-C2E21_1775	1.17	2.25 (up)	–	–	–	–	delta-aminolevulinic acid dehydratase
gene-C2E21_4366	1.25	2.37 (up)	–	–	−1.15	2.22 (down)	homogentisate chloroplastic, carotenoid biosynthetic process
gene-C2E21_5515	–	–	1.04	2.05 (up)	–	–	Carotene biosynthesis-related CBR
gene-C2E21_0737	1.13	2.19 (up)	–	–	–	–	cell division isoform B, photosystem II repair
gene-C2E21_9305	–	–	−1.11	2.15 (down)	–	–	photosystem II D1 precursor processing PSB27-chloroplastic isoform X1
gene-C2E21_4125	–	–	−2.46	5.49(down)	−2.53	5.79 (down)	Chlorophyll *a-b* binding chloroplastic
gene-C2E21_1397	–	–	1.25	2.38 (up)	–	–	Chlorophyll *a-b* binding of LHCII type chloroplastic
gene-C2E21_5933	–	–	−2.43	5.39 (down)	–	–	subunit of the chloroplast cytochrome *b6f* complex
gene-C2E21_7182	–	–	−1.24	2.37 (down)	–	–	Ferredoxin
gene-C2E21_5675	–	–	1.19	2.29 (up)	–	–	ferritin- chloroplastic
gene-C2E21_5085	2.26	4.81 (up)	2.13	4.36 (up)	–	–	Thioredoxin-like 1- chloroplastic
gene-C2E21_2271	−1.03	2.05 (down)	–	–	–	–	thioredoxin chloroplastic

"-" indicated "P-adjust > 0.05" or "not significantly different expressed" or "|log2FC|<1".

in both treatment CIP+/Col and CIP++/Col. The downregulated MFS transporter, whose function is to transport metals into and out of cells, is mainly classified as an efflux transporter protein (Khatiwada et al., 2020).

Differentially expressed genes related to metabolism

As previously mentioned, the presumed degradation process of CIP by *C. sorokiniana* mainly included a series of biochemical processes such as hydroxylation, oxidation and reduction. Thus, the gene expressions of metabolic enzymes involved might be changed. Because of the difference in CIP removal efficiency between different concentrations of CIP, DE-Gs between treatment CIP+/Col and CIP++/Col were also distinct. Cytochrome P450 and its isoform generally considered to be the key enzyme for oxidizing and metabolizing drugs were 2.07 and 2.24 times upregulated in treatment CIP++/Col (as shown in Table 4). Previous research verified that cytochrome P450 was involved in the metabolic process of CIP (Xie et al., 2020), and thus further explained the difference in removal efficiency between low and high concentrations of CIP. 2OG-Fe(II) oxygenase superfamily biochemically catalyzed hydroxylation, halogenation, desaturation, epimerization, cyclization, ring expansion, C-C bond cleavage, demethylation and so on (Jia et al., 2017a). Overexpression of gene associated might be inextricably linked to the degradation of CIP by *C. sorokiniana*, because it mainly relied on these reactions for bio-removal. Moreover, the expressions of various oxidoreductase genes in cells were obviously upregulated, including NADPH-dependent diflavin oxidoreductase 1 isoform X1, cysteine dioxygenase, NADP-dependent malate dehydrogenase, bifunctional acetaldehyde-alcohol dehydrogenase isoform B and ferric-chelate reductase. In addition, energy is critical in the transportation and metabolism of CIP. Thus, the expression of gene-C2E21_9142 and gene-C2E21_6345 (ATPase) were 2.03 and 2.40 times upregulated.

Conclusion

In this study, the growth conditions of *C. sorokiniana* under CIP stress and its removal were investigated through RNA-seq. The results showed that the growth of *C. sorokiniana* was not affected by changes in CIP concentration. The increase in humic acid in the extracellular environment of cells attenuated the toxic effects of CIP, and the upregulated expression of antioxidant substances and efflux pump helped to resist

Table 3. Differentially expressed genes related to transmembrane activity of *C. sorokiniana* induced by CIP

	CIP+/Col		CIP++/Col		CIP++/CIP+		
Gene ID	log2Fold change	Fold change	log2Fold change	Fold change	log2Fold change	Fold change	Annotations
gene-C2E21_3505	–	–	1.34	2.53 (up)	–	–	ABC transporter ATP-binding
gene-C2E21_1472	–	–	1.05	2.07 (up)	1.51	2.84 (up)	ABC transporter B family member 28 isoform X2
gene-C2E21_5763	−1.69	3.22 (down)	−1.13	2.18 (down)	–	–	MFS transporter
gene-C2E21_6330	1.42	2.67 (up)	1.43	2.69 (up)	–	–	zinc transporter
gene-C2E21_1856	1.00	2.00 (up)	2.00	3.99 (up)	–	–	zinc transporter
gene-C2E21_8904	–	–	1.78	3.43 (up)	1.45	2.73 (up)	Zinc (Zn2)-Iron (Fe2) Permease (ZIP) Family isoform A
gene-C2E21_1820	1.47	2.77 (up)	1.73	3.31 (up)	–	–	CTR type copper ion transporter
gene-C2E21_8394	–	–	1.27	2.41 (up)	–	–	voltage-gated ion channel superfamily
gene-C2E21_0103	–	–	−1.09	2.13 (down)	–	–	inactive cadmium zinc-transporting ATPase HMA3

"-" indicated "P-adjust > 0.05" or "not significantly different expressed" or "|log2FC|<1".

oxidative stress and reduce cellular damage from CIP, facilitating cells to adapt to the exposure of CIP and avoid cell death. The photosynthetic system was negatively affected under CIP stress, causing the decrease of OEC, ΦPSII and NPQ values of *C. sorokiniana*. In addition, CIP could be effectively removed by *C. sorokiniana* with the removal efficiency of 83.30% at 20 mg L^{-1}, and the biodegradation was the dominant removal mechanism in the algal cells. According to the metabolite identified by HPLC-MS/MS, the photolysis and biodegradation pathways of CIP by *C. sorokiniana* were proposed, which might orientate the future finding and further investigation in the biodegradation pathway of fluoroquinolone antibiotics. Furthermore, transcriptome sequencing results inferred the mechanism of CIP degradation by *C. sorokiniana*. ABC transporters might play an essential role in the transmembrane transport of CIP by *C. sorokiniana*. Intracellular CIP might experience the catabolic process of oxidative hydroxylation and ring opening mineralization by the cytochrome P450, 2OG-Fe(II) oxygenase superfamily, dioxygenase, etc. The activity of ATPase was enhanced, and more energy was obtained for the transport and degradation of CIP through hydrolysis of ATP. Future research could focus on ways to increase the removal of low concentrations of CIP. Besides, more investigation should be conducted about the key genes in the degradation of CIP.

Limitations of the study

One of the main limitations of the study is that the intermediates of CIP were speculated based on HPLC-MS/MS results and previous study. Future study may focus on chemically studying compounds contents of the system to determine main intermediates.

STAR★METHODS

Detailed methods are provided in the online version of this paper and include the following:

- KEY RESOURCES TABLE
- RESOURCE AVAILABILITY
  - Lead contact
  - Materials availability
  - Data and code availability
- EXPERIMENTAL MODEL AND SUBJECT DETAILS
  - Microbe strains
- METHOD DETAILS
  - Chemicals
  - Microalgae growth analysis
  - Analysis of photosynthetic parameters in response to CIP
  - Extracellular polymeric substance analysis

Table 4. Differentially expressed genes related to metabolism of *C. sorokiniana* induced by CIP

	CIP+/Col		CIP++/Col		CIP++/CIP+		
Gene ID	log2Fold change	Fold change	log2Fold change	Fold change	log2Fold change	Fold change	Annotations
gene-C2E21_2725	2.87	7.33 (up)	4.04	16.40 (up)	1.16	2.24 (up)	2OG-Fe(II) oxygenase superfamily
gene-C2E21_9291	1.00	2.00 (up)	1.14	2.20 (up)	–	–	NADPH-dependent diflavin oxidoreductase 1 isoform X1
gene-C2E21_7633	–	–	1.05	2.07 (up)	–	–	cytochrome P450
gene-C2E21_3034			1.17	2.24 (up)	1.31	2.48 (up)	cytochrome P450 55A3 isoform A
gene-C2E21_4846	–	–	2.31	4.94 (up)	2.14	4.42 (up)	cysteine dioxygenase
gene-C2E21_7353	–	–	1.11	2.16 (up)	1.21	2.31 (up)	NADP-dependent malate dehydrogenase
gene-C2E21_1830	–	–	1.17	2.25 (up)	1.61	3.04 (up)	bifunctional acetaldehyde- alcohol dehydrogenase isoform B
gene-C2E21_5734	–	–	1.06	2.09 (up)	–	–	ferric-chelate reductase
gene-C2E21_3542	–	–	−1.05	2.07 (down)	–	–	FAD-dependent oxidoreductase
gene-C2E21_3699	–	–	−1.17	2.25 (down)	–	–	NADPH:quinone reductase
gene-C2E21_9142	1.02	2.03 (up)	–	–	–	–	ATPase AAA
gene-C2E21_6345	–	–	1.26	2.40 (up)	–	–	ATPase family AAA domain-containing 2

"-" indicated "P-adjust > 0.05" or "not significantly different expressed" or "|log2FC|<1".

SUPPLEMENTAL INFORMATION

Supplemental information can be found online at https://doi.org/10.1016/j.isci.2022.104638.

ACKNOWLEDGMENTS

This work was financially supported by the National Key R&D program of China (2019YFC1803405; 2019YFD1101300).

AUTHOR CONTRIBUTIONS

Zhuo Li: Conceptualization, Data curation, Writing - original draft. Shuangxi Li: Data curation, Investigation. Tianrui Li: Investigation. Xinxin Gao: Investigation. Liandong Zhu: Conceptualization, Writing - original draft.

DECLARATION OF INTERESTS

The authors declare no competing interests.

INCLUSION AND DIVERSITY

The author list of this paper includes contributors from the location where the research was conducted who participated in the data collection, design, analysis, and/or interpretation of the work. While citing references scientifically relevant for this work, we also actively worked to promote gender balance in our reference list.

Received: January 15, 2022
Revised: April 9, 2022
Accepted: June 14, 2022
Published: July 15, 2022

REFERENCES

Abbew, A.-W., Qiu, S., Amadu, A.A., Qasim, M.Z., Chen, Z., Wu, Z., Wang, L., and Ge, S. (2021). Insights into the multi-targeted effects of free nitrous acid on the microalgae *Chlorella sorokiniana* in wastewater. Bioresour. Technol. *347*, 126389. https://doi.org/10.1016/j.biortech.2021.126389.

Adamiec, M., Gibasiewicz, K., Luciński, R., Giera, W., Chełminiak, P., Szewczyk, S., Sipińska, W., van Grondelle, R., and Jackowski, G. (2015). Excitation energy transfer and charge separation are affected in *Arabidopsis thaliana* mutants lacking light-harvesting chlorophyll *a/b* binding protein Lhcb3. J. Photochem. Photobiol. B Biol. *153*, 423–428. https://doi.org/10.1016/j.jphotobiol.2015.11.002.

Amaral, V., Romera-Castillo, C., García-Delgado, M., Gómez-Parra, A., and Forja, J. (2020). Distribution of dissolved organic matter in estuaries of the southern Iberian Atlantic Basin: sources, behavior and export to the coastal zone. Mar. Chem. *226*, 103857. https://doi.org/10.1016/j.marchem.2020.103857.

Antonacci, A., Celso, F.L., Barone, G., Calandra, P., Grunenberg, J., Moccia, M., Gatto, E., Giardi, M.T., and Scognamiglio, V. (2020). Novel atrazine-binding biomimetics inspired to the D1 protein from the photosystem II of Chlamydomonas reinhardtii. Int. J. Biol. Macromol. *163*, 817–823. https://doi.org/10.1016/j.ijbiomac.2020.07.010.

Aron, N.S.M., Khoo, K.S., Chew, K.W., Veeramuthu, A., Chang, J.-S., and Show, P.L. (2021). Microalgae cultivation in wastewater and potential processing strategies using solvent and membrane separation technologies. J. Water Proc. Eng. *39*, 101701. https://doi.org/10.1016/j.jwpe.2020.101701.

Bistarelli, L.T., Poyntner, C., Santín, C., Doerr, S.H., Talluto, M.V., Singer, G., and Sigmund, G. (2021). Wildfire-derived pyrogenic carbon modulates riverine organic matter and biofilm enzyme activities in an in situ flume experiment. ACS ES T Water *1*, 1648–1656. https://doi.org/10.1021/acsestwater.1c00185.

Brym, A., Paerl, H.W., Montgomery, M.T., Handsel, L.T., Ziervogel, K., and Osburn, C.L. (2014). Optical and chemical characterization of base-extracted particulate organic matter in coastal marine environments. Mar. Chem. *162*, 96–113. https://doi.org/10.1016/j.marchem.2014.03.006.

Chai, L., Huang, M., Fan, H., Wang, J., Jiang, D., Zhang, M., and Huang, Y. (2019). Urbanization altered regional soil organic matter quantity and quality: insight from excitation emission matrix (EEM) and parallel factor analysis (PARAFAC). Chemosphere *220*, 249–258. https://doi.org/10.1016/j.chemosphere.2018.12.132.

Cheah, W.Y., Show, P.L., Juan, J.C., Chang, J.-S., and Ling, T.C. (2018). Waste to energy: the effects of Pseudomonas sp on *Chlorella sorokiniana* biomass and lipid productions in palm oil mill effluent. Clean Technol. Environ. Policy *20*, 2037–2045. https://doi.org/10.1007/s10098-018-1505-7.

Chen, M.-M., Niu, H.-Y., Niu, C.-G., Guo, H., Liang, S., and Yang, Y.-Y. (2022). Metal-organic framework-derived CuCo/carbon as an efficient magnetic heterogeneous catalyst for persulfate activation and ciprofloxacin degradation. J. Hazard. Mater. *424*, 127196. https://doi.org/10.1016/j.jhazmat.2021.127196.

Chen, Z., Lai, W., Xu, Y., Xie, G., Hou, W., Zhanchang, P., Kuang, C., and Li, Y. (2021). Anodic oxidation of ciprofloxacin using different graphite felt anodes: kinetics and degradation pathways. J. Hazard. Mater. *405*, 124262. https://doi.org/10.1016/j.jhazmat.2020.124262.

Cheng, J., Ye, Q., Li, K., Liu, J., and Zhou, J. (2018). Removing ethinylestradiol from wastewater by microalgae mutant *Chlorella* PY-ZU1 with CO_2 fixation. Bioresour. Technol. *249*, 284–289. https://doi.org/10.1016/j.biortech.2017.10.036.

Cheng, J., Ye, Q., Yang, Z., Yang, W., Zhou, J., and Cen, K. (2017). Microstructure and antioxidative capacity of the microalgae mutant *Chlorella* PY-ZU1 during tilmicosin removal from wastewater under 15% CO_2. J. Hazard. Mater. *324*, 414–419. https://doi.org/10.1016/j.jhazmat.2016.11.006.

Du, X., Gu, L.-p., Wang, T.-t., Kou, H.-j., and Sun, Y. (2021). The relationship between the molecular composition of dissolved organic matter and bioavailability of digestate during anaerobic digestion process: characteristics, transformation and the key molecular interval. Bioresour. Technol. *342*, 125958. https://doi.org/10.1016/j.biortech.2021.125958.

Fick, J., Söderström, H., Lindberg, R.H., Phan, C., Tysklind, M., and Larsson, D.J. (2009). Contamination of surface, ground, and drinking water from pharmaceutical production. Environ. Toxicol. Chem. *28*, 2522–2527. https://doi.org/10.1897/09-073.1.

Gomaa, M., Zien-Elabdeen, A., Hifney, A.F., and Adam, M.S. (2021). Phycotoxicity of antibiotics and non-steroidal anti-inflammatory drugs to green algae *Chlorella* sp. and *Desmodesmus spinosus*: assessment of combined toxicity by Box-Behnken experimental design. Environ. Technol. Innovat. *23*, 101586. https://doi.org/10.1016/j.eti.2021.101586.

Gomes, T., Xie, L., Brede, D., Lind, O.-C., Solhaug, K.A., Salbu, B., and Tollefsen, K.E. (2017). Sensitivity of the green algae *Chlamydomonas reinhardtii* to gamma radiation: photosynthetic performance and ROS formation. Aquat. Toxicol. *183*, 1–10. https://doi.org/10.1016/j.aquatox.2016.12.001.

Gothwal, R., and Shashidhar. (2017). Occurrence of high levels of fluoroquinolones in aquatic environment due to effluent discharges from bulk drug manufacturers. J. Hazard. Toxic. Radioact. Waste *21*. https://doi.org/10.1061/(asce)hz.2153-5515.0000346.

Hagenbuch, I.M., and Pinckney, J.L. (2012). Toxic effect of the combined antibiotics ciprofloxacin, lincomycin, and tylosin on two species of marine diatoms. Water Res. *46*, 5028–5036. https://doi.org/10.1016/j.watres.2012.06.040.

He, Q., Chen, L., Zhang, S., Chen, R., Wang, H., Zhang, W., and Song, J. (2018). Natural sunlight induced rapid formation of water-born algal-bacterial granules in an aerobic bacterial granular photo-sequencing batch reactor. J. Hazard. Mater. *359*, 222–230. https://doi.org/10.1016/j.jhazmat.2018.07.051.

Homem, V., and Santos, L. (2011). Degradation and removal methods of antibiotics from aqueous matrices - a review. J. Environ. Manag. *92*, 2304–2347. https://doi.org/10.1016/j.jenvman.2011.05.023.

Huguet, A., Vacher, L., Relexans, S., Saubusse, S., Froidefond, J.M., and Parlanti, E. (2009). Properties of fluorescent dissolved organic matter in the Gironde Estuary. Org. Geochem. *40*, 706–719. https://doi.org/10.1016/j.orggeochem.2009.03.002.

Jia, B., Jia, X., Kim, K.H., and Jeon, C.O. (2017a). Integrative view of 2-oxoglutarate/Fe(II)-dependent oxygenase diversity and functions in bacteria. Biochim. Biophys. Acta Gen. Subj. *1861*, 323–334. https://doi.org/10.1016/j.bbagen.2016.12.001.

Jia, F., Yang, Q., Liu, X., Li, X., Li, B., Zhang, L., and Peng, Y. (2017b). Stratification of extracellular polymeric substances (EPS) for aggregated anammox microorganisms. Environ. Sci. Technol. *51*, 3260–3268. https://doi.org/10.1021/acs.est.6b05761.

Juneau, P., El Berdey, A., and Popovic, R. (2002). PAM fluorometry in the determination of the sensitivity of *Chlorella vulgaris, Selenastrum capricornutum*, and *Chlamydomonas reinhardtii* to copper. Arch. Environ. Contam. Toxicol. *42*, 155–164. https://doi.org/10.1007/s00244-001-0027-0.

Khatiwada, B., Hasan, M.T., Sun, A., Kamath, K.S., Mirzaei, M., Sunna, A., and Nevalainen, H. (2020). Proteomic response of *Euglena gracilis* to heavy metal exposure - identification of key proteins involved in heavy metal tolerance and accumulation. Algal Res. *45*, 101764. https://doi.org/10.1016/j.algal.2019.101764.

Kiran, B.R., and Venkata Mohan, S. (2021). Photosynthetic transients in *Chlorella sorokiniana* during phycoremediation of dairy wastewater under distinct light intensities. Bioresour. Technol. *340*, 125593. https://doi.org/10.1016/j.biortech.2021.125593.

Kumar, K.S., Dahms, H.-U., Lee, J.-S., Kim, H.C., Lee, W.C., and Shin, K.-H. (2014). Algal photosynthetic responses to toxic metals and herbicides assessed by chlorophyll a fluorescence. Ecotoxicol. Environ. Saf. *104*, 51–71. https://doi.org/10.1016/j.ecoenv.2014.01.042.

Kumar, S., Kaushik, R.D., and Purohit, L.P. (2022). ZnO-CdO nanocomposites incorporated with graphene oxide nanosheets for efficient photocatalytic degradation of bisphenol A, thymol blue and ciprofloxacin. J. Hazard Mater. *424*, 127332. https://doi.org/10.1016/j.jhazmat.2021.127332.

Kusvuran, S. (2021). Microalgae (*Chlorella vulgaris* Beijerinck) alleviates drought stress of broccoli plants by improving nutrient uptake, secondary metabolites, and antioxidative defense system. Hortic. Plant J. *7*, 221–231. https://doi.org/10.1016/j.hpj.2021.03.007.

Lambrev, P.H., Miloslavina, Y., Jahns, P., and Holzwarth, A.R. (2012). On the relationship

between non-photochemical quenching and photoprotection of Photosystem II. Biochim. Biophys. Acta Bioenerg. *1817*, 760–769. https://doi.org/10.1016/j.bbabio.2012.02.002.

Larsson, D.J., de Pedro, C., and Paxeus, N. (2007). Effluent from drug manufactures contains extremely high levels of pharmaceuticals. J. Hazard. Mater. *148*, 751–755. https://doi.org/10.1016/j.jhazmat.2007.07.008.

Li, S., and Hu, J. (2018). Transformation products formation of ciprofloxacin in UVA/LED and UVA/LED/TiO_2 systems: impact of natural organic matter characteristics. Water Res. *132*, 320–330. https://doi.org/10.1016/j.watres.2017.12.065.

Li, S., Chu, R., Hu, D., Yin, Z., Mo, F., Hu, T., Liu, C., and Zhu, L. (2020a). Combined effects of 17 beta-estradiol and copper on growth, biochemical characteristics and pollutant removals of freshwater microalgae *Scenedesmus dimorphus*. Sci. Total Environ. *730*, 138597. https://doi.org/10.1016/j.scitotenv.2020.138597.

Li, S., Huang, T., Du, P., Liu, W., and Hu, J. (2020b). Photocatalytic transformation fate and toxicity of ciprofloxacin related to dissociation species: experimental and theoretical evidences. Water Res. *185*, 116286. https://doi.org/10.1016/j.watres.2020.116286.

Li, S., Wang, P., Zhang, C., Zhou, X., Yin, Z., Hu, T., Hu, D., Liu, C., and Zhu, L. (2020c). Influence of polystyrene microplastics on the growth, photosynthetic efficiency and aggregation of freshwater microalgae *Chlamydomonas reinhardtii*. Sci. Total Environ. *714*, 136767. https://doi.org/10.1016/j.scitotenv.2020.136767.

Li, X., Yang, C., Zeng, G., Wu, S., Lin, Y., Zhou, Q., Lou, W., Du, C., Nie, L., and Zhong, Y. (2020d). Nutrient removal from swine wastewater with growing microalgae at various zinc concentrations. Algal Res. *46*, 101804. https://doi.org/10.1016/j.algal.2020.101804.

Liao, L., Chen, S., Peng, H., Yin, H., Ye, J., Liu, Z., Dang, Z., and Liu, Z. (2015). Biosorption and biodegradation of pyrene by *Brevibacillus brevis* and cellular responses to pyrene treatment. Ecotoxicol. Environ. Saf. *115*, 166–173. https://doi.org/10.1016/j.ecoenv.2015.02.015.

Liu, N., Zhang, H., Zhao, J., Xu, Y., and Ge, F. (2020). Mechanisms of cetyltrimethyl ammonium chloride-induced toxicity to photosystem II oxygen evolution complex of *Chlorella vulgaris* F1068. J. Hazard. Mater. *383*, 121063. https://doi.org/10.1016/j.jhazmat.2019.121063.

Lovyagina, E.R., and Semin, B.K. (2016). Mechanism of inhibition and decoupling of oxygen evolution from electron transfer in photosystem II by fluoride, ammonia and acetate. J. Photochem. Photobiol. B Biol. *158*, 145–153. https://doi.org/10.1016/j.jphotobiol.2016.02.031.

Lu, P., Lin, K., and Gan, J. (2020). Enhanced ozonation of ciprofloxacin in the presence of bromide: kinetics, products, pathways, and toxicity. Water Res. *183*, 116105. https://doi.org/10.1016/j.watres.2020.116105.

Ma, Z.K., Chu, D.T.W., Cooper, C.S., Li, Q., Fung, A.K.L., Wang, S.Y., Shen, L.L., Flamm, R.K., Nilius, A.M., Alder, J.D., et al. (1999). Synthesis and antimicrobial activity of 4*H*-4-Oxoquinolizine derivatives: consequences of structural modification at the C-8 position. J. Med. Chem. *42*, 4202–4213. https://doi.org/10.1021/jm990191k.

Maia, A.S., Ribeiro, A.R., Amorim, C.L., Barreiro, J.C., Cass, Q.B., Castro, P.M.L., and Tiritan, M.E. (2014). Degradation of fluoroquinolone antibiotics and identification of metabolites/transformation products by liquid chromatography-tandem mass spectrometry. J. Chromatogr. A *1333*, 87–98. https://doi.org/10.1016/j.chroma.2014.01.069.

Murphy, K.R., Stedmon, C.A., Graeber, D., and Bro, R. (2013). Fluorescence spectroscopy and multi-way techniques. PARAFAC. Anal. Methods *5*, 6557. https://doi.org/10.1039/c3ay41160e.

Nie, X.P., Wang, X., Chen, J., Zitko, V., and An, T. (2008). Response of the freshwater alga *Chlorella vulgaris* to trichloroisocyanuric acid and ciprofloxacin. Environ. Toxicol. Chem. *27*, 168. https://doi.org/10.1897/07-028.1.

Oberoi, A.S., Jia, Y., Zhang, H., Khanal, S.K., and Lu, H. (2019). Insights into the fate and removal of antibiotics in engineered biological treatment systems: a critical review. Environ. Sci. Technol. *53*, 7234–7264. https://doi.org/10.1021/acs.est.9b01131.

Peng, J., He, Y.-Y., Zhang, Z.-Y., Chen, X.-Z., Jiang, Y.-L., Guo, H., Yuan, J.-P., and Wang, J.-H. (2022). Removal of levofloxacin by an oleaginous microalgae *Chromochloris zofingiensis* in the heterotrophic mode of cultivation: removal performance and mechanism. J. Hazard. Mater. *425*, 128036. https://doi.org/10.1016/j.jhazmat.2021.128036.

Phoon, B.L., Ong, C.C., Mohamed Saheed, M.S., Show, P.-L., Chang, J.-S., Ling, T.C., Lam, S.S., and Juan, J.C. (2020). Conventional and emerging technologies for removal of antibiotics from wastewater. J. Hazard. Mater. *400*, 122961. https://doi.org/10.1016/j.jhazmat.2020.122961.

Rodriguez-Mozaz, S., Chamorro, S., Marti, E., Huerta, B., Gros, M., Sànchez-Melsió, A., Borrego, C.M., Barceló, D., and Balcázar, J.L. (2015). Occurrence of antibiotics and antibiotic resistance genes in hospital and urban wastewaters and their impact on the receiving river. Water Res. *69*, 234–242. https://doi.org/10.1016/j.watres.2014.11.021.

Santana, M.A., Tan, F.C., and Smith, A.G. (2002). Molecular characterisation of coproporphyrinogen oxidase from *Glycine max* and *Arabidopsis thaliana*. Plant Physiol. Biochem. *40*, 289–298. https://doi.org/10.1016/s0981-9428(02)01374-8.

Stingley, R.L., Khan, A.A., and Cerniglia, C.E. (2004). Molecular characterization of a phenanthrene degradation pathway in *Mycobacterium vanbaalenii* PYR-1. Biochem. Biophys. Res. Commun. *322*, 133–146. https://doi.org/10.1016/j.bbrc.2004.07.089.

Tang, S., Yin, H., Yu, X., Chen, S., Lu, G., and Dang, Z. (2021). Transcriptome profiling of *Pseudomonas aeruginosa* YH reveals mechanisms of 2, 2′, 4, 4′-tetrabrominated diphenyl ether tolerance and biotransformation. J. Hazard. Mater. *403*, 124038. https://doi.org/10.1016/j.jhazmat.2020.124038.

Tian, Y.-n., Zhong, R.-h., Wei, J.-b., Luo, H.-h., Eyal, Y., Jin, H.-l., Wu, L.-j., Liang, K.-y., Li, Y.-m., Chen, S.-z., et al. (2021). *Arabidopsis* CHLOROPHYLLASE 1 protects young leaves from long-term photodamage by facilitating FtsH-mediated D1 degradation in photosystem II repair. Mol. Plant *14*, 1149–1167. https://doi.org/10.1016/j.molp.2021.04.006.

Van Doorslaer, X., Dewulf, J., Van Langenhove, H., and Demeestere, K. (2014). Fluoroquinolone antibiotics: an emerging class of environmental micropollutants. Sci. Total Environ. *500–501*, 250–269. https://doi.org/10.1016/j.scitotenv.2014.08.075.

Wang, H., Abassi, S., and Ki, J.-S. (2019). Origin and roles of a novel copper-zinc superoxide dismutase (CuZnSOD) gene from the harmful dinoflagellate *Prorocentrum minimum*. Gene *683*, 113–122. https://doi.org/10.1016/j.gene.2018.10.013.

Wei, L., Li, H., and Lu, J. (2021). Algae-induced photodegradation of antibiotics: a review. Environ. Pollut. *272*, 115589. https://doi.org/10.1016/j.envpol.2020.115589.

Westerhoff, P., Yoon, Y., Snyder, S., and Wert, E. (2005). Fate of endocrine-disruptor, pharmaceutical, and personal care product chemicals during simulated drinking water treatment processes. Environ. Sci. Technol. *39*, 6649–6663. https://doi.org/10.1021/es0484799.

Xiao, G., Chen, J., Show, P.L., Yang, Q., Ke, J., Zhao, Q., Guo, R., and Liu, Y. (2021). Evaluating the application of antibiotic treatment using algae-algae/activated sludge system. Chemosphere *282*, 130966. https://doi.org/10.1016/j.chemosphere.2021.130966.

Xie, P., Chen, C., Zhang, C., Su, G., Ren, N., and Ho, S.-H. (2020). Revealing the role of adsorption in ciprofloxacin and sulfadiazine elimination routes in microalgae. Water Res. *172*, 115475. https://doi.org/10.1016/j.watres.2020.115475.

Xie, P., Ho, S.-H., Peng, J., Xu, X.-J., Chen, C., Zhang, Z.-F., Lee, D.-J., and Ren, N.-Q. (2019). Dual purpose microalgae-based biorefinery for treating pharmaceuticals and personal care products (PPCPs) residues and biodiesel production. Sci. Total Environ. *688*, 253–261. https://doi.org/10.1016/j.scitotenv.2019.06.062.

Xiong, J.-Q., Kurade, M.B., and Jeon, B.-H. (2018). Can microalgae remove pharmaceutical contaminants from water? Trends Biotechnol. *36*, 30–44. https://doi.org/10.1016/j.tibtech.2017.09.003.

Xiong, J.-Q., Kurade, M.B., Kim, J.R., Roh, H.-S., and Jeon, B.-H. (2017). Ciprofloxacin toxicity and its co-metabolic removal by a freshwater microalga *Chlamydomonas mexicana*. J. Hazard. Mater. *323*, 212–219. https://doi.org/10.1016/j.jhazmat.2016.04.073.

Xu, H., Cai, H., Yu, G., and Jiang, H. (2013). Insights into extracellular polymeric substances of cyanobacterium *Microcystis aeruginosa* using fractionation procedure and parallel factor analysis. Water Res. *47*, 2005–2014. https://doi.org/10.1016/j.watres.2013.01.019.

Yamashita, Y., Kloeppel, B.D., Knoepp, J., Zausen, G.L., and Jaffé, R. (2011). Effects of watershed history on dissolved organic matter

characteristics in headwater streams. Ecosystems *14*, 1110–1122. https://doi.org/10.1007/s10021-011-9469-z.

You, X., Cao, X., Zhang, X., Guo, J., and Sun, W. (2021). Unraveling individual and combined toxicity of nano/microplastics and ciprofloxacin to *Synechocystis* sp. at the cellular and molecular levels. Environ. Int. *157*, 106842. https://doi.org/10.1016/j.envint.2021.106842.

Yun, C.-J., Hwang, K.-O., Han, S.-S., and Ri, H.-G. (2019). The effect of salinity stress on the biofuel production potential of freshwater microalgae *Chlorella vulgaris* YH703. Biomass Bioenergy *127*. https://doi.org/10.1016/j.biombioe.2019.105277.

Zhang, H., Xu, Z., Huo, Y., Guo, K., Wang, Y., He, G., Sun, H., Li, M., Li, X., Xu, N., and Sun, G. (2020). Overexpression of *Trx* CDSP32 gene promotes chlorophyll synthesis and photosynthetic electron transfer and alleviates cadmium-induced photo-inhibition of PSII and PSI in tobacco leaves. J. Hazard. Mater. *398*, 122899. https://doi.org/10.1016/j.jhazmat.2020.122899.

Zhao, X., Hu, Z., Yang, X., Cai, X., Wang, Z., and Xie, X. (2019). Noncovalent interactions between fluoroquinolone antibiotics with dissolved organic matter: a ^{1}H NMR binding site study and multi-spectroscopic methods. Environ. Pollut. *248*, 815–822. https://doi.org/10.1016/j.envpol.2019.02.077.

Zhao, Z., Yang, X., Cai, W., Lei, Z., Shimizu, K., Zhang, Z., Utsumi, M., and Lee, D.-J. (2018). Response of algal-bacterial granular system to low carbon wastewater: focus on granular stability, nutrients removal and accumulation. Bioresour. Technol. *268*, 221–229. https://doi.org/10.1016/j.biortech.2018.07.114.

Zhou, G.-J., Ying, G.-G., Liu, S., Zhou, L.-J., Chen, Z.-F., and Peng, F.-Q. (2014). Simultaneous removal of inorganic and organic compounds in wastewater by freshwater green microalgae. Environ. Sci. Process. Impacts *16*, 2018. https://doi.org/10.1039/c4em00094c.

Zhou, J.S., Hao, D.Y., Wang, X.D., Liu, T.M., He, C.Y., Xie, F., Sun, Y.H., and Zhang, J. (2006). An important role of a "probable ATP-binding component of ABC transporter" during the process of *Pseudomonas aeruginosa* resistance to fluoroquinolone. Proteomics *6*, 2495–2503. https://doi.org/10.1002/pmic.200501354.

STAR★METHODS

KEY RESOURCES TABLE

REAGENT or RESOURCE	SOURCE	IDENTIFIER
Biological samples		
Chlorella sorokiniana	The Institute of Hydrobiology, Chinese Academy of Sciences	Cat#FACHB-25
Chemicals, peptides, and recombinant proteins		
Ciprofloxacin	Shanghai Macklin Biochemical Co.,Ltd.	Cat#C11901815; CAS:85,721-33-1
Sodium hydroxide	Sinopharm Chemical Reagent	Cat#10019762; CAS:1319-73-2
Acetone	Shanghai lingfeng chemical reeagent Co.,Ltd.	CAS:67-64-1
Acetonitrile	Fisher chemical	Cat#A998-4; CAS:75-05-8
Formic acid	Sinopharm Chemical Reagent	Cat#10010118; CAS:64-18-6
Critical commercial assays		
TRIzol® Reagent	Invitrogen	Cat#15596018
DNase I	DNase I	Cat#2270A
TruSeqTM RNA sample preparation Kit	Illumina	Cat#RS-200-0012
Super-Script double-stranded cDNA synthesis kit	Invitrogen	Cat#11917020
Software and algorithms		
UV–VIS spectrophotometer	Shimadzu	UV-2600
Portable microalgae fluorescence meter	AquaPen	AquaPen-C AP 110-C
MATLAB R2021a	MathWorks	https://www.mathworks.com/products/get-matlab.html?s_tid=gn_getml
drEEM toolbox	Murphy et al., (2013)	http://dreem.openfluor.org/
Spectrophotometer FS5	Edinburgh Instruments Ltd.	FS5
High-performance liquid chromatography (HPLC)	Agilent	Agilent Technologies 1200 Series
HPLC column	Agilent	Eclipse XDB-C_{18} column (5 μm, 4.6 × 250 mm)
Liquid Chromatography High Resolution Mass Spectrometer	Absciex	TripleQTOF5600+
2100 Bioanalyser	Agilent	G2939AA
NanoDrop Technologies	Thermo Scientific	ND-2000
IBM SPSS Statistics 20	IBM	https://www.ibm.com/support/pages/node/723799
Origin 2020	OriginLab	https://www.originlab.com/index.aspx?go=PRODUCTS/OriginStudentVersion

RESOURCE AVAILABILITY

Lead contact

Further information and requests for resources and reagents should be directed to and will be fulfilled by the lead contact, Zhuo Li (zhuoli2000@whu.edu.cn).

Materials availability

This study did not generate new unique reagents.

Data and code availability

This study did not generate any unique datasets. All data generated during this study are either supplied in the figures and the supplemental information or will be shared by the lead contact upon request. This paper does not report original code.

Any additional information required to reanalyze the data reported in this paper is available from the lead contact upon request.

EXPERIMENTAL MODEL AND SUBJECT DETAILS

Microbe strains

Chlorella sorokiniana, provided by the Institute of Hydrobiology, Chinese Academy of Sciences, was cultivated in the medium of autoclaved BG-11 nutrient media at the pH of 7.2 in a conical flask of 100 mL. The BG-11 medium was purchased from Qingdao Hope Bio-Technology Co,.Ltd., consisting of $NaNO_3$ (1.5 g L^{-1}), K_2HPO_4 (0.04 g L^{-1}), $MgSO_4{\cdot}7H_2O$ (0.075 g L^{-1}), $CaCl_2{\cdot}2H_2O$ (0.036 g L^{-1}), citric acid (0.006 g L^{-1}), ferric ammonium citrate (0.006 g L^{-1}), $Na_2{\cdot}EDTA$ (0.001 g L^{-1}), Na_2CO_3 (0.02 g L^{-1}) and 1.0 mL of trace metal solution per liter. The trace metal includes H_3BO_3 (2.86 g L^{-1}), $MnCl_4{\cdot}4H_2O$ (1.86 g L^{-1}), $ZnSO_4{\cdot}7H_2O$ (0.22 g L^{-1}), $CuSO_4{\cdot}5H_2O$ (0.08 g L^{-1}), $Na_2MoO_4{\cdot}4H_2O$ (0.39 g L^{-1}) and $Co(NO_3){\cdot}6H_2O$ (0.05 g L^{-1}). Under an appropriate light condition of 200 μmol/m^2 (light-to-dark ratio 12 h/12 h) and suitable temperate of 28°C, the microalgal culture was manually shaken four times a day to avoid the growth of microalgae cells along the flask wall.

To examine the effect of CIP and its removal efficiency by *C. sorokiniana*, exponentially growing microalgae cells were exposed to media composed of different CIP concentrations of 1, 5, 10 and 20 mg L^{-1}. Besides, a series of batch experiments were conducted to investigate the elimination routes of CIP at 20 mg L^{-1}. The microalgal elimination routes for CIP were considered to be photolysis, hydrolysis and bioremoval. Photolysis and hydrolysis tests were conducted to investigate their contribution during CIP removal process.

METHOD DETAILS

Chemicals

CIP was purchased from Shanghai Macklin Biochemical Co., Ltd. 2 g L^{-1} stock solution of CIP was prepared using weak alkaline solution (0.02% w/w NaOH). Then, the CIP solution was subjected to filtration sterilization through a 0.22 μm membrane filter. Other reagents used in this study are analytical or HPLC grade.

Microalgae growth analysis

The optical density of the microalgae sample was analyzed using a UV–2600 spectrophotometer (Shimadzu, Japan) at 680 nm (OD_{680}). The linear relationship between OD_{680} and the cell dry weigh of *C. sorokiniana* (DW) was established, and the standard curve was calculated by Equation (1):

$$DW\ (g/L) = 0.1672 \times OD_{680} - 0.0015 \quad \text{(Equation 1)}$$

In the study, specific growth rate was used to describe the change in biomass concentration over time. The specific growth rate (μ) was determined by the range of correlation points in the exponential growth period of microalgae, based on the relationship between ln(DW) and time, which was described by Equation (2).

$$\mu = \frac{ln(DW_i/DW_0)}{t_i/t_0} \quad \text{(Equation 2)}$$

where DW_i and DW_0 correspond to the dry weight of microalgae biomass at time t_i and t_0, respectively.

Analysis of photosynthetic parameters in response to CIP

The contents of chlorophyll *a* and *b* as well as carotenoid were analyzed using the methods of a previous study (Li et al., 2020a). Specifically, 8 mL algal culture was obtained and centrifuged at 4°C, 8000 rpm for 10 min. Then, the supernatant was removed and 8 mL 90% acetone was added into centrifugal tubes. The microalgal suspension was placed in a refrigerator for dark treatment at 4°C for 24 h, and subsequently was centrifuged at 4°C, 8000 rpm for 10 min. The supernatants were measured at absorbance of 470, 652 and 665 nm by the UV–2600 spectrophotometer. The concentrations of chlorophyll *a*, *b* and carotenoid were calculated by the following Equations (3), (4), and (5):

$$\text{Chl a } (mg/L) = 16.72 \times OD_{665} - 9.16 \times OD_{652} \quad \text{(Equation 3)}$$

$$\text{Chl b } (mg/L) = 34.09 \times OD_{652} - 15.28 \times OD_{665} \quad \text{(Equation 4)}$$

$$\text{Carotenoid } (mg/L) = \left(1000 \times OD_{470} - 1.63 \times Chlorophyll\ a\right)/221 \quad \text{(Equation 5)}$$

The contents of photosynthetic pigments were expressed as mg g^{-1} by dividing the concentration of each pigment by dry weight of *C. sorokiniana*.

Chlorophyll fluorescence parameter was measured by a portable microalgae fluorescence meter (Aquapen 110-C, Czech Republic). 3 mL algae culture was obtained and dark-adapted for at least for 20 min, thereby performing photosynthesis, according to the manufacturer's operating manual (Li et al., 2020c). Four chlorophyll fluorescence parameters were analyzed, based on the operating program data, including F_v/F_m and efficiency of OEC, ΦPSII and NPQ.

Calculated as following Equation (6), F_v/F_m reflected the maximum quantum efficiency of photosystem II, while OEC reflecting the efficiency of the oxygen-evolving complex, calculated as following Equation (7) (Liu et al., 2020):

$$F_v/F_m = \frac{F_m - F_0}{F_m} \quad \text{(Equation 6)}$$

$$\text{OEC} = \frac{F_0}{F_m - F_0} \quad \text{(Equation 7)}$$

where F_m and F_o are the maximum and minimum fluorescence in dark-adapted state, respectively.

As one of the most important parameters that revealed the physiological state, ΦPSII measured the efficiency of PSII photochemistry and was calculated as following Equation (8):

$$\Phi\text{PSII} = \frac{F'_m - F_t}{F'_m} \quad \text{(Equation 8)}$$

Non-photochemical quenching (NPQ) was quantified using the maximum fluorescence measured in the dark-adapted sample by Equation (9) (Kiran and Mohan, 2021):

$$\text{NPQ} = \frac{F_m - F'_m}{F'_m} \quad \text{(Equation 9)}$$

Extracellular polymeric substance analysis

The characterization of dissolved organic matter (DOM) was determined by the combined use of three-dimensional excitation-emission matrix (EEM) and parallel factor analysis (PARAFAC) (Murphy et al., 2013). All algal samples were centrifuged and the supernatants were passed through 0.45 mm membrane filters before measurement. Subsequently, they were measured by a fluorescence spectrophotometer (FS_5, Edinburgh Instruments Ltd., England), equipped with a pulsed xenon lamp (150 W). The scan ranges were set from 200 to 500 nm for excitation (Ex) with 5-nm sampling intervals, and the emission (Em) spectra from 250 to 600 nm were obtained in 1 nm increments. The Ex and Em slit bandwidths were set as 5 and 1 nm, respectively. A PARAFAC analysis was performed in MATLAB (Version 2020, MathWorks, USA) using the drEEM toolbox to separate the different fluorescent components of the DOM.

The verified excitation and emission loadings are used as a precondition to model the un-scaled data, and then multiply by the maximum excitation and emission loadings to obtain the maximum fluorescence (F_{max}) of each component in Raman. According to the method described by Chai et al. (2019), Humic Index (HIX) and Biological Index (BIX) were calculated based on EEM spectrum as follows:

$$\text{HIX} = \sum I_{em\ 434-480nm} \Big/ \left(\sum I_{em\ 300-344nm} + \sum I_{em\ 434-480nm}\right)(\lambda_{ex\ 254nm}) \quad \text{(Equation 10)}$$

$$\text{BIX} = I_{em\ 380nm}/I_{em\ 430nm}(\lambda_{ex\ 310nm}) \quad \text{(Equation 11)}$$

where I_{em} and λ_{ex} are emission and excitation intensity at different wavelengths.

CIP removal analysis

Microalgal culture (5 mL) was sampled daily to determine the residual concentration of CIP. The culture media were centrifuged at 4°C, 8000 rpm for 10 min to separate the microalgal cells, and the supernatants

were filtered through 0.45 μm membrane filters. The concentrations of CIP in different groups were analyzed by high performance liquid chromatography (HPLC, Agilent Technologies 1200 Series, Agilent, USA) under 269 nm. 20 μL of supernatant was injected into an Eclipse XDB-C_{18} column (5 μm, 4.6 × 250 mm, Agilent) at 30°C. The mobile phase was acetonitrile/ultrapure water with 0.1% (v/v) formic acid (25/75, v/v) at a flow rate of 1 mL/min. The retention time of CIP was 2.816 min under this chromatographic analysis conditions.

CIP intermediates were identified using the Liquid Chromatography High Resolution Mass Spectrometer (Absciex). The intermediates obtained include both photolytic and biodegradation pathways in the biodegradation experiments. The mobile phase of HPLC conditions was gradient elution mode (shown in Table S5) with a flow rate at 0.4 mL min^{-1} in Kinetic C18 column (100 mm × 2.1 mm, 2.6 μm). Accurate MS patterns of CIP and its biodegradation products, were analyzed in negative ionization scanning mode (m/z 100 to 1000).

Transcriptome analysis

20 mL of culture media was exposed to 5 and 10 mg L^{-1} CIP for 10 days, and control groups were centrifuged and the cells were collected. Total RNA was extracted from the tissue using TRIzol® Reagent, according to the manufacturer's instructions (Invitrogen), and genomic DNA was removed using DNase I (TaKara). Then, RNA quality was determined by 2100 Bioanalyser (Agilent) and quantified using the ND-2000 (NanoDrop Technologies). Only high-quality RNA sample (OD260/280 = 1.8~2.2, OD260/230 ≥ 2.0, RIN≥6.5, 28S:18S ≥ 1.0, >1μg) was used to construct sequencing library.

RNA-seq transcriptome library was prepared following TruSeqTM RNA sample preparation Kit from Illumina (San Diego, CA) using 1 μg of total RNA. Messenger RNA was isolated and synthesized double-stranded cDNA by using a SuperScript double-stranded cDNA synthesis kit (Invitrogen, CA) with random hexamer primers (Illumina). Then, the synthesized cDNA was subjected to end-repair, phosphorylation and 'A' base addition. Libraries were size selected for cDNA target fragments of 300 bp, followed by PCR amplification. Then RNA-seq sequencing library was sequenced.

The clean reads obtained for 9 samples were first mapped to the *Chlorella sorokiniana* reference genome GCA_002245835.2 (https://www.ncbi.nlm.nih.gov/genome/31394?genome_assembly_id=367175). The gene expression level was first standardized by calculating transcripts per kilobase per million mapped reads (TPM). DEGs expression analysis was performed by DESeq2 with false discovery rate correction (FDR) P-adjusted ≤0.05, while DEGs with |log2FC|>1 and P-adjusted ≤0.05 were considered to be significantly different expressed genes.

QUANTIFICATION AND STATISTICAL ANALYSIS

All the experiments were carried out in triplicates and results were presented as means ±standard error. One-way analysis of variance(ANOVA) followed by Tukey's HSD Post Hoc multiple comparison analysis was conducted by IBM SPSS 20 to analysis the significant differences between different experimental groups. Values were considered significant at $P < 0.05$.